Ultramicroscopy 000 (2017) 1–12

Contents lists available at ScienceDirect

Ultramicroscopy

journal homepage: www.elsevier.com/locate/ultramic

The impact of STEM aberration correction on materials science

Stephen J. Pennycook

Department of Materials Science and Engineering, National University of Singapore, Singapore

ARTICLE INFO

Article history:
Received 12 October 2016
Revised 4 March 2017
Accepted 16 March 2017
Available online xxx

Keywords:
Scanning transmission electron microscope
Incoherent imaging
Z-contrast
Atomic resolution
Aberration correction

ABSTRACT

Over the last three decades the scanning transmission electron microscope (STEM) has gone from a specialized instrument for nanoscale analysis to the microscope of choice for atomic resolution imaging of materials, allowing incoherent high-angle annular dark field (Z-contrast) imaging, coherent phase contrast modes (conventional and annular bright field), electron energy loss and energy dispersive X-ray spectroscopy. All signals are achieving atomic resolution and several are available simultaneously. This would not have been possible without the development of an aberration corrector for the STEM, spearheaded by Ondrej Krivanek in the late 1990s, which finally allowed the benefits of the STEM to translate from "in-principle" to actual daily practice. Here I will recall my own experiences with the aberration-corrected STEM in partnership with Ondrej, a truly exciting and rewarding journey.

1. Introduction

This account is largely my personal view on how aberration correction on the STEM has transformed the field of electron microscopy. Let's start with a brief history of the STEM (for a more detailed account of the development see [1]). The potential benefits have long been appreciated; Manfred von Ardenne invented the STEM in 1938 [2,3], following Ernst Ruska's invention of the TEM in 1932 [4], because he realized that the STEM did not need to refocus transmitted electrons back into an image, and therefore would not be hampered by chromatic aberration in the same way as the TEM. However, his first images immediately revealed the Achilles heel of STEM, noise. It was not possible to get enough current into the probe to form a good quality image and von Ardenne gave up the STEM in favor of the TEM [5].

It is Albert Crewe who is commonly regarded as the father of the modern STEM. Not only did he invent the cold field emission gun which enabled orders of magnitude more current in the probe [6], he also understood the benefits in placing the critical optics before the sample, and advocated the use of a spectrometer to collect the inelastic scattering [7]. A few years later the annular dark field (ADF) detector appeared and the first direct images of individual single heavy atoms were reported [8]. The term Z-contrast made its appearance, referring to a ratio image between the elastic (ADF) and inelastic signals, which, for single atoms, is proportional to atomic number Z [9]. The technique became widely used in the biological sciences for mass measurement [10–12], but was not useful in most materials applications because of strong diffraction contrast effects which masked any Z-contrast [13].

To overcome the strong diffraction contrast required higher scattering angles be collected, when coherent Bragg scattering would be replaced with incoherently generated thermal diffuse scattering [14–17]. This was my introduction to Z-contrast imaging. At that time, as a student in the Cavendish Laboratory I was working on cathodoluminescence, which is also an incoherently generated signal [18–20]. Michael Treacy wanted to try his ideas on imaging with high angle Rutherford scattering and we modified my cathodoluminescence detector accordingly, obtaining the first HAADF images of catalysts which showed the anticipated improved visibility and reduced Bragg contrast, as shown in Fig. 1 [21–24].

In 1982 I joined Oak Ridge National Laboratory as a staff member in the group of Jagdish Narayan and started to apply the Z-contrast technique to ion-implanted semiconductors. Again, the changeover from diffraction contrast imaging of structure to Z-contrast imaging of the implanted dopants was striking [25], see Fig. 2. I began to wonder what the image would look like with an atomic sized probe; surely in thin enough crystals we would have to see a direct Z-contrast structure image [26]? The Department of Energy granted me the chance to investigate further with a VG Microscopes HB501UX equipped with a high resolution pole piece and a set of masks to exclude low angle scattering from the annular detector. In the summer of 1988 I obtained what I thought were the first incoherent, Z-contrast images at atomic resolution [27], see Fig. 3. It was only later I discovered that John Cowley at Arizona State University had published a STEM bright field and ADF image of $Ti_2Nb_{10}O_{29}$, using a VG Microscopes HB5 [28]. He commented on the enhanced resolution of the dark field image but did

E-mail address: steve.pennycook@nus.edu.sg

http://dx.doi.org/10.1016/j.ultramic.2017.03.020
0304-3991/

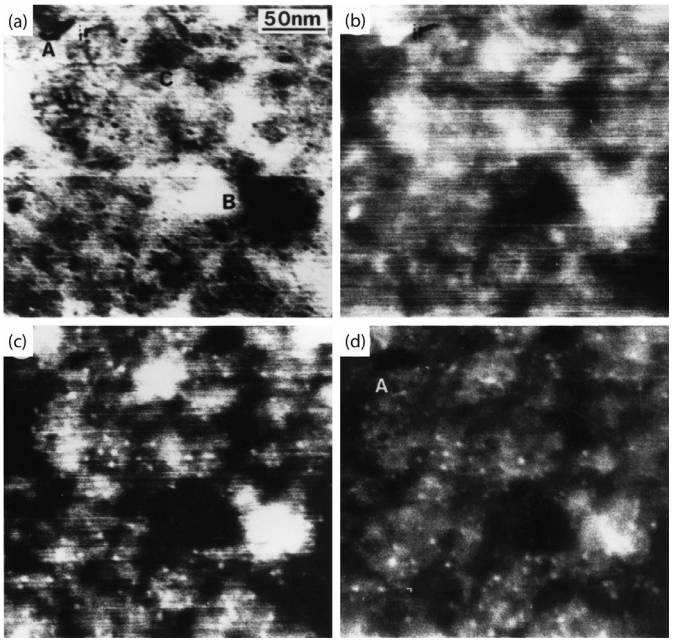

Fig. 1. Images of Pt particles on γ-alumina recorded in (a) bright field, (b) low angle ADF, (c) HAADF and (d) the ratio of high angle to low angle ADF signals. Particle contrast is highest in the HAADF image, reproduced from M. M. J. Treacy, PhD thesis, University of Cambridge, 1979.

not mention if the image showed other incoherent characteristics, such as no contrast reversals. These characteristics had been predicted previously by Engel based on simulations of single atoms [29]. The most surprising feature of the HAADF images was perhaps the thickness dependence, which also showed predominantly incoherent characteristics. Instead of thickness fringes or contrast reversals as in bright field imaging, the HAADF images showed no obvious change in form, just a slowly decreasing contrast with increasing thickness, see Fig. 4.

The physical explanation lay in the fact that the high angle scattering came predominantly from just the highly localized 1 s type Bloch states [30–37]. In coherent high-resolution TEM (HRTEM) all Bloch states interfere to form the image and the strong thickness dependence results. Only in very thin crystals can the image be interpreted as a structure image, a good example being Ondrej's famous study of a Ge grain boundary by high voltage TEM [38]. For most materials, especially at lower voltages, image interpretation required construction of candidate model structures, simulations of possible images as a function of defocus and thickness, and finding the best fit. The problem of course is that there is no guarantee that the actual structure would be thought of. The Z-contrast image, being incoherent in nature, immediately suggested the likely structure, and most interfaces were actually found to be more complex than previously imagined. An excellent example is shown in Fig. 5, where Z-contrast imaging of an ultrathin $(Si_4Ge_8)_{24}$ superlattice reveals strong interfacial ordering which indicated an unexpected step-driven atom pump mechanism [39]. Images of superlattices in high-temperature superconductors revealed a much simpler cell-by-cell growth mechanism, see Fig. 6 [40,41].

While these images are noisy with low resolution and poor contrast by today's standards, the incoherent characteristics were clear. The STEM just needed to wait for advances in engineering, in particular the aberration corrector. And so the of field high resolution imaging began the gradual conversion from the TEM to the STEM. Some key milestones along the way include, first, the installation of a 300 kV VG Microscopes HB603U STEM in Oak Ridge with a high resolution pole piece that enabled resolution of the dumbbell in Si [42] and GaAs [43], allowing the sublattice polarity to be seen by inspection, see Fig. 7. Second, the achievement of atomic-resolution EELS [44,45], where the simultaneous, atomic-resolution Z-contrast image unambiguously located the probe position with respect to the atom columns. Third, the development

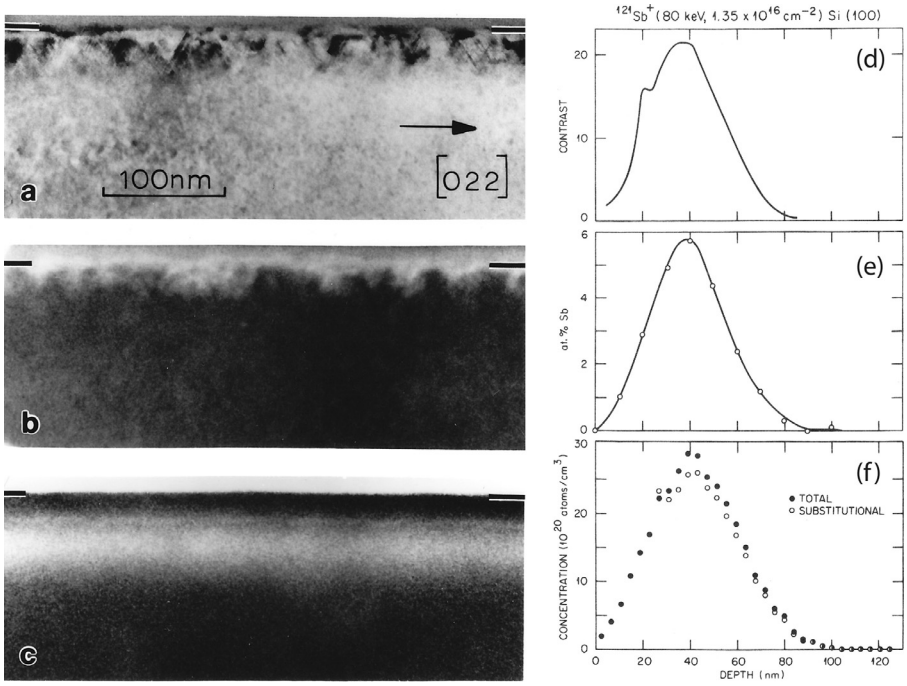

Fig. 2. Cross section images of Sb implanted Si. (a) TEM diffraction contrast image showing defects near the surface and end of range damage, (b) a low angle ADF image also dominated by diffraction contrast, (c) a HAADF image revealing the Sb profile (d), in agreement with (e) X-ray microanalysis and (f) Rutherford backscattering spectroscopy, reproduced from [25].

Please cite this article as: S.J. Pennycook, The impact of STEM aberration correction on materials science, Ultramicroscopy (2017), http://dx.doi.org/10.1016/j.ultramic.2017.03.020

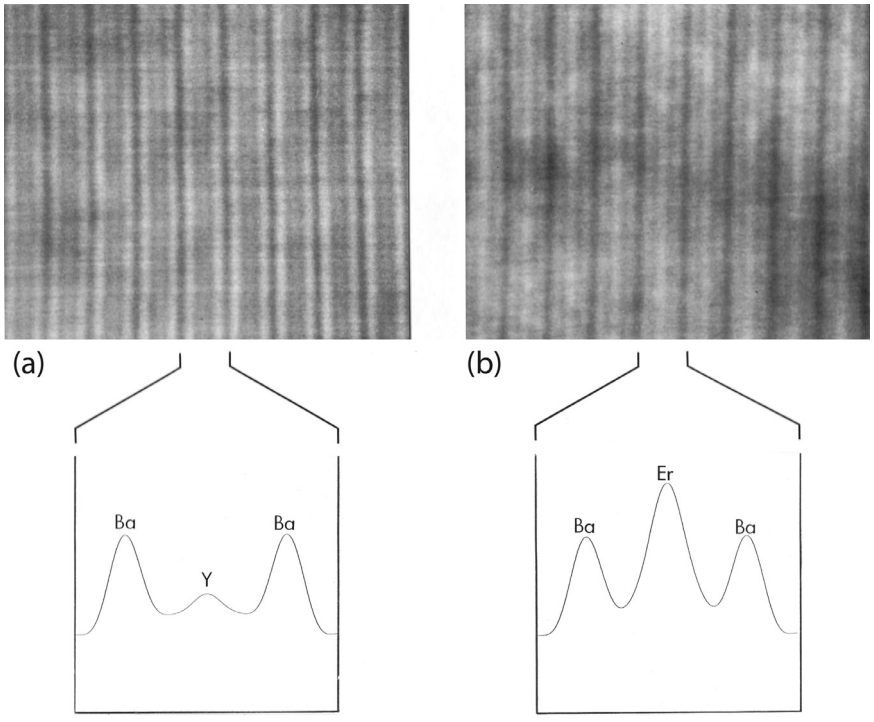

Fig. 3. HAADF images in a planar channeling condition from (a) $YBa_2Cu_3O_{7-\delta}$ and (b) $ErBa_2Cu_3O_{7-\delta}$, with calculated intensity profiles across each unit cell. The expected strong Z-contrast closely matches the experimental result, reproduced from [27].

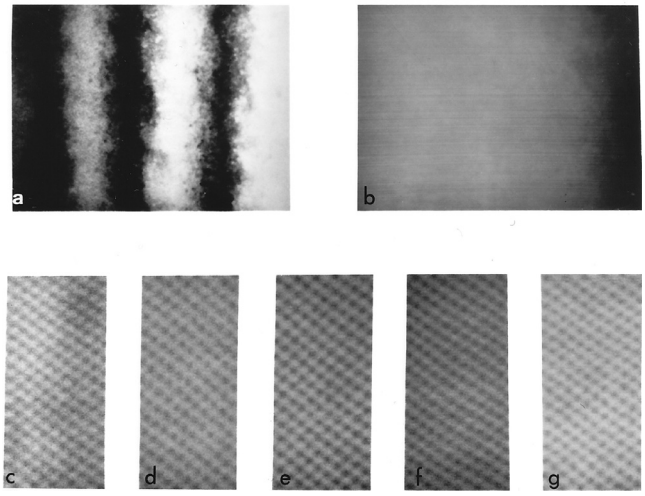

Fig. 4. Simultaneously recorded (a) bright field and (b) HAADF images of Si in the ⟨110⟩ zone axis using an objective aperture too small to allow bright field lattice images. In this case the bright field image shows thickness fringes allowing the Z-contrast image to be measured as a function of sample thickness, (c–g), reproduced from [31].

of an atomic-resolution STEM by a large commercial manufacturer, JEOL, with a 2010F purchased by Nigel Browning at the University of Illinois, Chicago [46]. Ondrej himself mirrors this transition. When I first met him he was about to leave the Metal Physics group at the Cavendish and I was an incoming student. He had already become a legend in the group through his studies of amorphous materials through HRTEM [47] and his method for measuring the coefficient of spherical aberration (C_S) [48]. He went to Japan, and produced the grain boundary structure image with the high voltage microscope [38], then to the University of California, Berkeley, still using conventional HRTEM [49], but after joining Arizona State University he became interested in EELS [50].

Later Ondrej joined the Gatan company where he introduced their parallel detection EEL spectrometer [51]. In a visit to the Orsay group he demonstrates single atom detectability on their HB501 STEM [52]. In this paper he mentions that reducing the C_S by a factor of three would "improve the visibility of heavy atoms such as thorium considerably," referring to an ADF image. As parallel detection spectrometers use multipole lenses, which are one way to correct spherical aberration [53], we can see that Ondrej probably already had his sights on aberration correction. He develops the imaging filter with more complex multipole lenses [54], then in 1995 leaves Gatan to work on aberration correction at the Cavendish Laboratory, using the same VG HB5 microscope I had used for my thesis work almost 20 years earlier.

2. Aberration correction for incoherent imaging

Clearly by this time Ondrej had decided that his future would focus on STEM, in contrast to the German aberration correction project that was primarily TEM based [55,56]. The question of who achieved what first has been discussed recently [57–59], but it was during this time my own path crossed Ondrej's again. The Oak Ridge HB501UX by this time was ageing, not used much for imaging after the installation of the 300 kV HB603, but was still used for EELS since the 300 kV machine had no spectrometer at that time [60]. Together with Niklas Dellby, Ondrej founded the Nion company (initially named Colibris) to supply Philip Batson, IBM, with an aberration corrector for his HB501. I was rather easily persuaded to apply for funds to do likewise, and also to install a corrector in the HB603U. Ondrej delivered: with Batson he achieved the first sub-Ångstrom STEM probe [61] and with the Oak Ridge group, and Peter Nellist, we achieved the first sub-Ångstrom resolution of a crystal lattice using the 300 kV microscope [62], see Fig. 8. Maria Varela achieved the first spectroscopic identification of a single atom within a bulk crystal with the rejuvenated 100 kV microscope [63]. This microscope now had the resolution of the uncorrected 300 kV machine [64].

Please cite this article as: S.J. Pennycook, The impact of STEM aberration correction on materials science, Ultramicroscopy (2017), http://dx.doi.org/10.1016/j.ultramic.2017.03.020

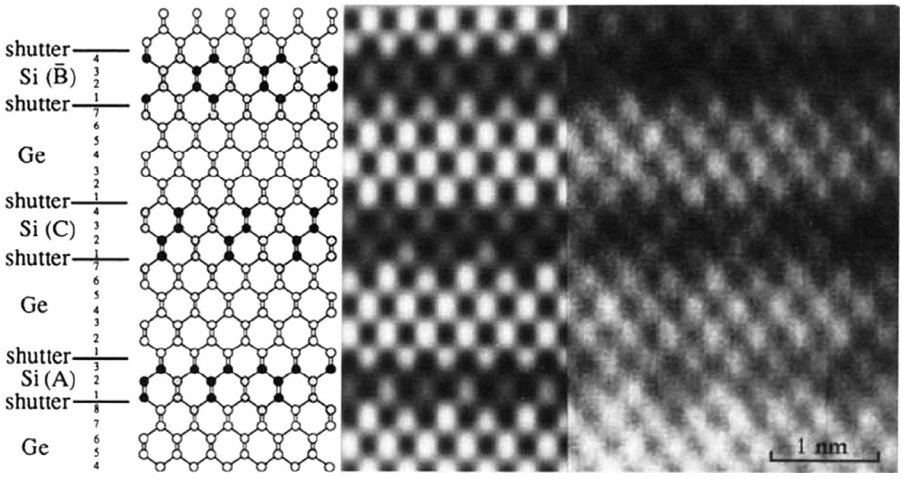

Fig. 5. [110] Z-contrast STEM image of a nominal $(Si_4Ge_8)_{24}$ superlattice showing interfacial ordering with simulated images of various ordered structures arising from the atom pump model. The [001] growth direction is toward the top of the image. Open circles represent Ge columns; solid circles, Si columns; and shaded circles, alloy columns. Simulation parameters are $C_S = 1.3$ mm, convergence angle = 10.3 mrad, and defocus = −69.4 nm. Reproduced from [39].

Fig. 9 shows the dramatic improvement in the ability of the HB603U to image single Pt catalyst atoms on γ-alumina after installation of the Nion aberration corrector [65,66]. Many materials advances rapidly ensued. For example, rare-earth sites in the intergranular phase of alumina were finally revealed [67,68], the origin of enhanced critical currents in Ca-doped $YBa_2Cu_3O_{7-x}$ grain boundaries was elucidated [69], interfacial stacking sequences in complex oxide heterostructures could be resolved for the first time [70,71] and nucleation sites of quantum wells were imaged [72]. For numerous other applications see the review articles from that period [73–76].

Prior to this experience there were a number of misgivings about the potential usefulness of aberration-corrected STEM. For example, would the smaller probe lead to so much more beam damage it would not be practical? Would the reduced depth of focus become an issue? Well it turns out that having a smaller probe means that for the same beam current the peak intensity is higher, giving better signal to noise ratio, and for a given crystal spacing the contrast is improved, basically a win-win situation. So smaller currents can be used with aberration corrected probes and beam damage is less important. Similarly with the reduced depth of field, if channeling is not too strong a focal series becomes a series of images from different depths, giving information on the 3D structure of the material [77,78]. While the depth resolution did not match that of tilt-series tomography, the lateral resolution, being at the atomic level, was far superior. The 3D location of individual Hf atoms in a high-dielectric constant gate stack was able to be achieved, see Fig. 10, [79,80] explaining the high leakage current [81].

Another unexpected gain was in bright field phase contrast imaging. Prior to aberration correction, the collector aperture size for coherent bright field imaging needed to be very small, performing the function of the condenser aperture in HRTEM [82,83]. Hence bright field images used only a small fraction of the probe current and were very noisy. However, with aberration correction the collector aperture could be increased an order of magnitude giving bright field images comparable to those that could be obtained by HRTEM. In STEM, however, coherent and incoherent images could be obtained simultaneously, with highly complementary characteristics, see Fig. 11 [75,84].

Even the traditional applications of STEM to microanalysis benefitted substantially. The aberration corrector does not necessarily need to be used to produce smaller probes, it can also be used to provide more current into the same sized probe, with great benefits for the weaker analytical signals, as predicted explicitly by Ondrej, [85] and later demonstrated experimentally [86–88].

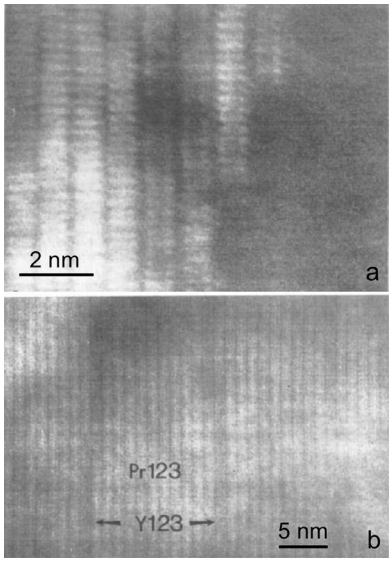

Fig. 6. (a) Z-contrast image of an amorphous/crystal interface in ion-implanted $YBa_2Cu_3O_{7-x}$ revealing the preferred crystal termination at the Cu-chain plane (dark lines). (b) Z-contrast image of a 1×8 $YBa_2Cu_3O_{7-x}/PrBa_2Cu_3O_{7-x}$ superlattice revealing the two-dimensional cell-by-cell growth mechanism (growth direction is to the right). Adapted from [40,41].

Of course, the CEOS corrector could also be used as a probe corrector [89,90] and they were in increasing demand from the large manufacturers, resulting in a rapid increase in STEM use. Another complementary imaging mode appeared, annular bright field (ABF) originally proposed by Rose [91], which is more efficient in imaging light elements [92-94]. In this way even H-atom columns could be seen in VH_2 [95,96]. Although it is a phase contrast image, it is quite incoherent in nature since it integrates over substantial regions of the probe-forming aperture. It is especially useful for measuring octahedral tilts in complex oxides [97].

Ondrej's choice to develop the aberration corrector for the STEM had really paid off. The STEM had finally overcome the historical noise issue that had plagued it for its entire history, and its inherent benefits could finally be exploited for applications, the interpretability of the incoherent image and the benefits of simulta-

Please cite this article as: S.J. Pennycook, The impact of STEM aberration correction on materials science, Ultramicroscopy (2017), http://dx.doi.org/10.1016/j.ultramic.2017.03.020

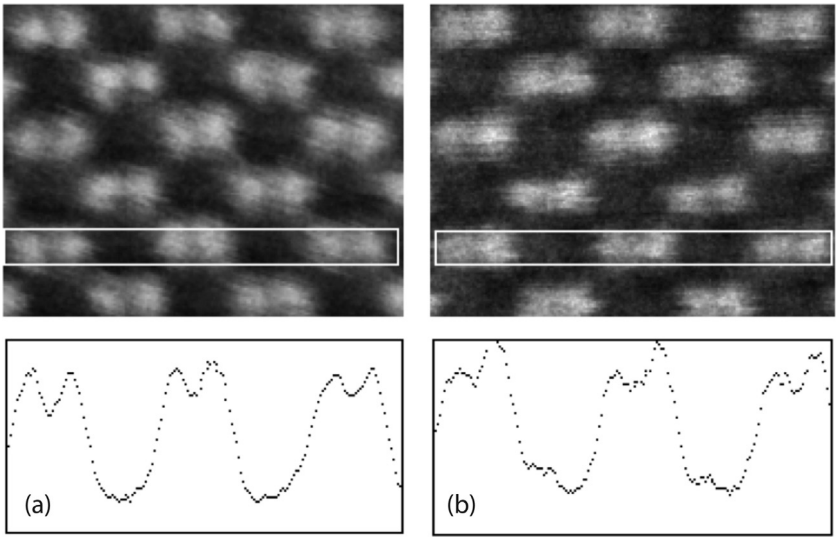

Fig. 7. Sublattice sensitivity in a 300 kV VG Microscopes HB603U STEM. Z-contrast images of (a) Si and (b) GaAs with line traces averaged vertically within the white rectangles, adapted from [43].

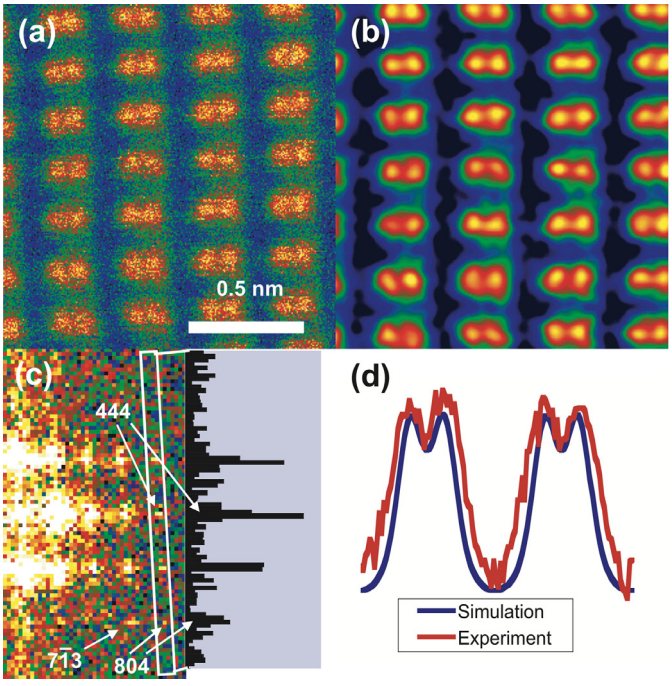

Fig. 8. (a) Image of Si [112] recorded using a VG Microscopes HB603U with Nion aberration corrector operating at 300 kV. (b) Image after low-pass filtering and unwarping. (c) Modulus of the Fourier transform and a profile of the region shown showing the 444 spacing (78 pm) of the dumbbell and evidence of information transfer at the (804) 61 pm spacing. (d) An intensity profile through two column pairs in (a) formed by summing over a width of 10 pixels with a simulated profile. Reproduced from [62].

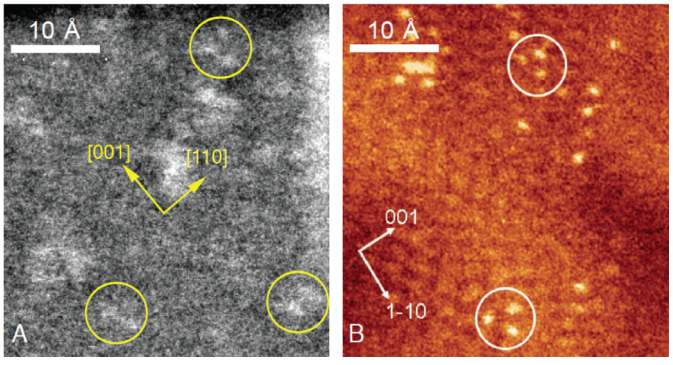

Fig. 9. Imaging of Pt atoms on γ-alumina with a VG Microscopes HB603U 300 kV STEM (a) before and (b) after aberration correction. Some Pt trimers and dimers are just visible in (a) but individual atoms are much more visible in (b). Images reproduced from (a) [65], (b) [66].

neous analytical signals. But an incoherent image has other benefits too, it has an intrinsically higher resolution than coherent HRTEM [98,99]. Over the next several years the STEM progressively broke resolution records to below 0.5 Å [91–94]. Only recently has the HREM method achieved similar performance, but requiring a 1200 kV acceleration voltage [100].

3. The UltraSTEM

Clearly installing correctors on old VG Microscopes columns was not optimum for demonstrating their performance, as the columns were never designed for such resolution. Peter Nellist joined Nion in 2000 to work on a 5th-order aberration corrector, which became incorporated in Ondrej's new UHV column - the UltraSTEM [85]. Ondrej also appreciated that contamination was a major issue in many columns and designed his new column to be fully bakeable. At Oak Ridge the VG Microscopes columns were having increasing issues with failures and stability. DOE was again persuaded to invest in a new microscope, and an UltraSTEM was acquired, with newly improved stabilized power supplies. Ondrej provided the perfect test sample, monolayer BN, and we achieved the first atom-by-atom identification of B, C, N and O directly from the intensity in the ADF image, see Fig. 12 [101]. Finally, through aberration correction, a Z-contrast image was not just for heavy atoms. It was another good demonstration of the power of incoherent imaging since it was very difficult to distinguish these light elements based on coherent images due to the similarity in atomic scattering factors [102]. In the Z-contrast image however the scattering cross section of O is over double that of B allowing a reliable identification even in the presence of noise (Fig. 12c).

The UltraSTEM used a VG Microscopes gun, with modified electronics, but represented a new trend in atomic resolution imaging: The use of lower acceleration voltages, which Ondrej termed "Gentle STEM" [103]. With graphene for example, 60 kV was well below the knock-on damage threshold and intrinsic defects could

Please cite this article as: S.J. Pennycook, The impact of STEM aberration correction on materials science, Ultramicroscopy (2017), http://dx.doi.org/10.1016/j.ultramic.2017.03.020

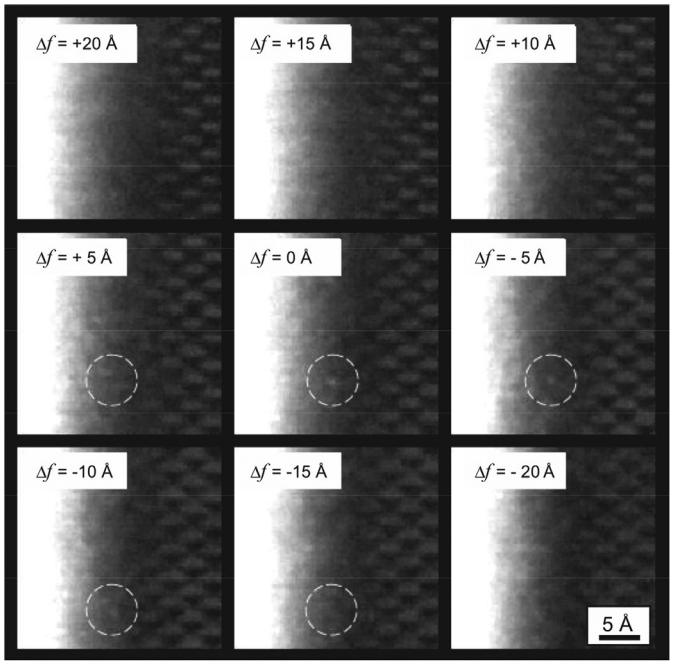

Fig. 10. A sequence of frames from a through-focal series of Z-contrast images of a $Si/SiO_2/HfO_2$ high-k device structure showing an individual Hf atom coming in and out of focus (circled). Results obtained with the aberration-corrected HB603, adapted from [79].

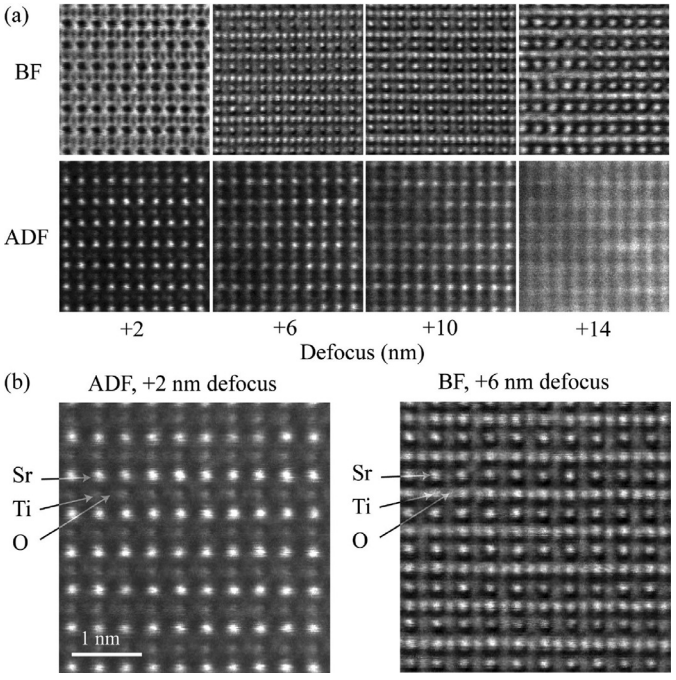

Fig. 11. Comparison of incoherent and coherent imaging of $SrTiO_3$ in the ⟨110⟩ projection using a 300 kV VG Microscopes' HB603U STEM with Nion aberration corrector. (a) A through focal series with 4 nm defocus steps in which the phase contrast images show complex variations in contrast while the incoherent ADF image contrast slowly blurs. All images are raw data and show some instabilities. (b) Under optimum conditions, the phase contrast BF image shows the O columns with high contrast while the ADF image shows the Sr columns brightest, the Ti columns less bright and O barely visible. Microscope parameters are optimized for the smallest probe with, nominally, a probe-forming aperture of ~ 22 mrad, C_s ~ – 0.037 mm and C_5 ~ 100 mm. Adapted from [171].

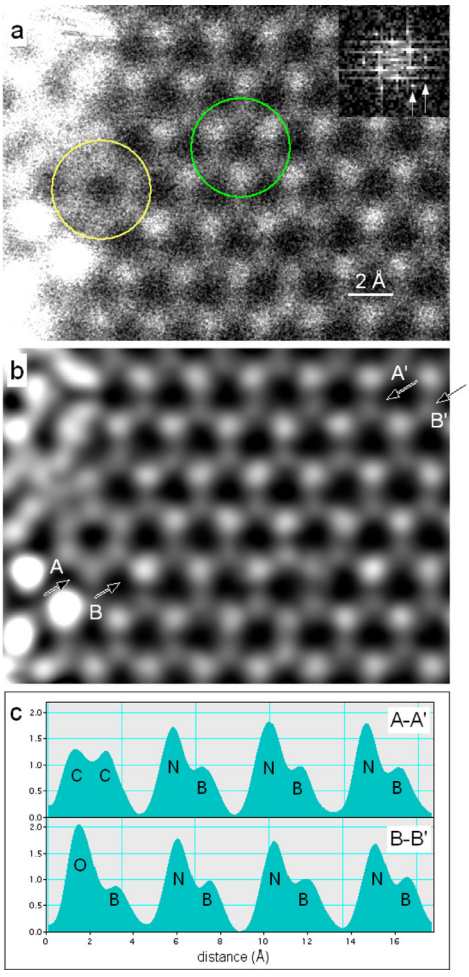

Fig. 12. (a) Raw ADF image of BN taken at an accelerating voltage of 60 kV. (b) Image corrected for distortion, smoothed and deconvolved to remove probe tails. (c) Line profiles between the indicated arrows shown on (b). Note that O atoms show over twice the intensity of B atoms. Reproduced from [101].

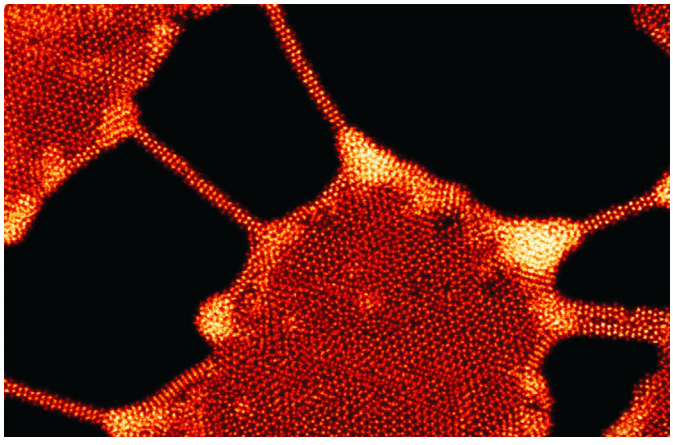

Fig. 13. Controlled nanofabrication of MoSe nanowire network from a $MoSe_2$ monolayer by electron beam nanofabrication, adapted from [108].

be studied more easily. Even so, atoms at edges and defects are more weakly bonded and could be knocked into metastable configurations. However, this provides information on the stability of the metastable configurations and has provided much insight into atomic dynamics of nanostructures [104–112], and even allows nanofabrication by electron beams, see Fig. 13 [108]. With

Please cite this article as: S.J. Pennycook, The impact of STEM aberration correction on materials science, Ultramicroscopy (2017), http://dx.doi.org/10.1016/j.ultramic.2017.03.020

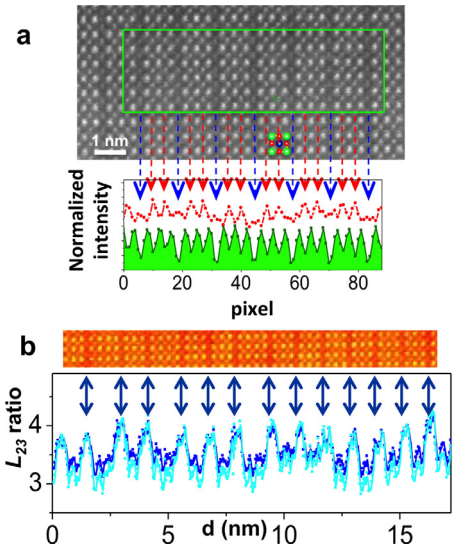

Fig. 14. (a) High resolution Z-contrast image of an LCO film showing dark stripes with an average modulation length of three perovskite blocks. EELS line traces vertically averaged within the green box show reduction of O from the dark stripes, green, La M_5 edge, red, O K edge. (b) EELS fine structure across the O-vacancy superlattice. Co L_3/L_2 intensity ratio calculated by using a Hartree-Slater cross-section step function (dark blue points), and also using the second derivative method (cyan dots). The top HAADF image shows the area where the line scan was acquired, blue arrows marking the O-deficient planes. Reproduced from [122]. (For interpretation of the references to color in this figure legend, the reader is referred to the web version of this article.)

the rapidly increasing interest in 2D materials the UltraSTEM was highly sought after, its simultaneous efficient ADF and EELS imaging providing quantitative insights into vacancies and defect configurations [113–117]. It also produced numerous new insights into the properties of complex oxide thin films, particularly on the role of oxygen vacancies, which were found to form ordered arrays as a strain relief mechanism but with dramatic effects on film properties, see for example Fig. 14 [118–122].

Ondrej also designed his own gun, using an innovative design to cover both low and high accelerating voltages up to 200 kV, which was delivered to Oak Ridge in the form of the UltraSTEM200. Easily capable of sub-Å resolution, it gave much better images of thicker materials such as CdSe solar cells, clearly revealing the atomic structure and Cl dopant segregation, see Fig. 15 [123–125]. Its higher energy beam also gave sufficient energy transfer to allow the direct imaging of atomic diffusion inside crystals, see Fig. 16 [126]. Quantitative matching of image contrast showed the diffusing Ce atoms to be inside the AlN crystal while density functional calculations revealed the energy barriers.

This was an exciting time for the Oak Ridge group and its many visitors, as we found new applications at both low and high beam energies. We also found new physics, for example, that the energy loss fine structure was dependent on probe position [127] necessitating incorporation of probe position and full solid state bonding effects into the matrix elements [128,129]. Also that large momentum transfer losses at low energy could show atomic resolution, again confirmed by density functional theory [130].

Ondrej's next project was his monochromator, an innovative design coupling the power supplies for the monochromator and the spectrometer for improved stability [131]. A spectacular energy resolution of only 9 meV was obtained using the Rutgers UltraSTEM, including a redesigned EELS filter, power supplies and detector in addition to the new monochromator. This simultaneous monochromator and spectrometer development allowed vibrational spectroscopy to be achieved in the STEM [132]. Again the EELS signal comprises high and low resolution components with theoretical predictions of atomic resolution being possible [133,134].

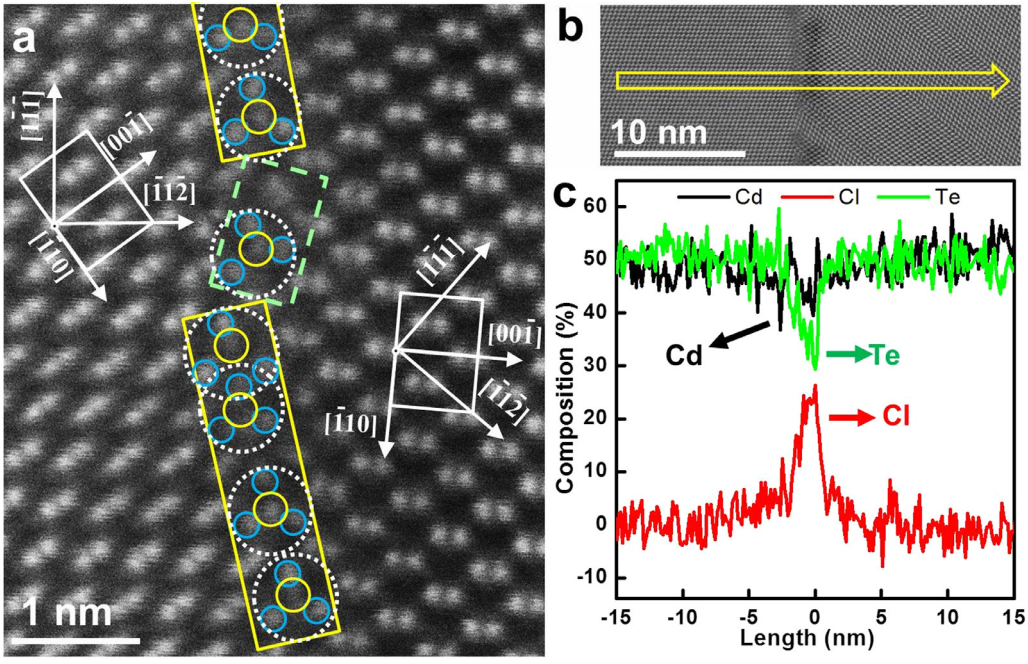

Fig. 15. Atomic structure and elemental distribution at a grain boundary in a $CdCl_2$-treated CdTe solar cell. (a) STEM Z-contrast image showing a Σ9 grain boundary with symmetric and asymmetric segments indicated by yellow and green dashed boxes, both comprising the same structural units, Cd_3Te dislocation cores (white dashed circles). The small blue and large yellow solid circles indicate single Cd and Te columns, respectively. (b) An EELS line scan was taken along the yellow arrow, and (c) the resulting composition profiles show strong Cl enrichment and Te reduction confined to a 1~2 nm range at the GB. Reproduced from [125]. (For interpretation of the references to color in this figure legend, the reader is referred to the web version of this article.)

Please cite this article as: S.J. Pennycook, The impact of STEM aberration correction on materials science, Ultramicroscopy (2017), http://dx.doi.org/10.1016/j.ultramic.2017.03.020

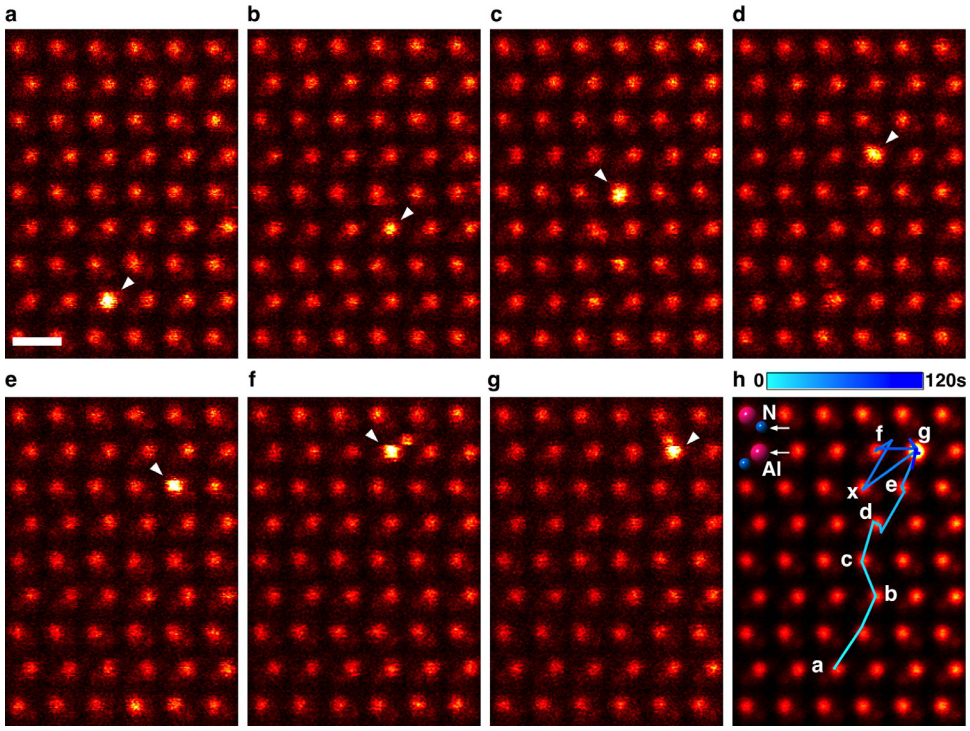

Fig. 16. Selected frames from a sequence of 30 Z-contrast images of a *w*-AlN single crystal doped with Ce viewed along the [11$\bar{2}$0] axis. (a–g), Frames 1, 4, 5, 6, 10, 16, 20, respectively, show the locations of a single Ce dopant as marked by the arrowhead in each panel. (h), Frame-averaged Z-contrast image. The observed Ce trace is overlaid and the Ce positions in each panel (a–g) are indicated. The scale bar is 3 Å. Reproduced from [126].

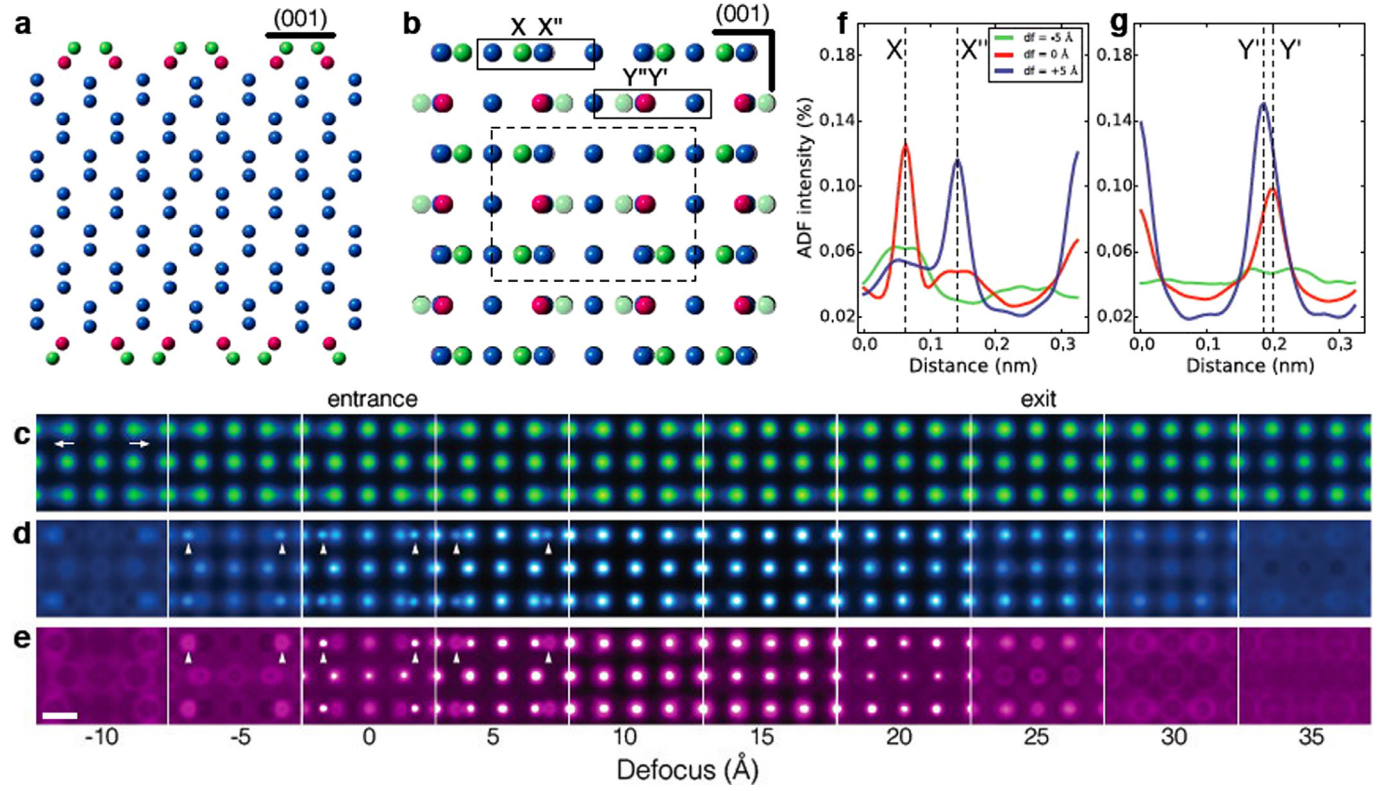

Fig. 17. The relaxed Si (001) surface atomic structure viewed along the (a) [100] and (b) [001] directions. The green-, red- and blue-colored Si atoms are positioned at the top-, sub-surface and bulk layers, respectively. Simulated focal-series ADF STEM images with (c) $\alpha = 30$ mrad at 200 kV, (d) $\alpha = 60$ mrad at 300 kV and (e) $\alpha = 100$ mrad at 300 kV. Note the changing relative intensity of the arrowed atoms. The focus range is −10 to 35 Å with 5 Å steps. Z-contrast intensity profiles obtained from the (f) X-X' and (e) Y"-Y' regions shown in (b) for the 100 mrad illumination with defocus of −5, 0, +5 Å. The scale bar in (e) is 2 Å. Reproduced from [170]. (For interpretation of the references to color in this figure legend, the reader is referred to the web version of this article.)

Please cite this article as: S.J. Pennycook, The impact of STEM aberration correction on materials science, Ultramicroscopy (2017), http://dx.doi.org/10.1016/j.ultramic.2017.03.020

4. Reflections

It has been a very rewarding journey with Ondrej seeing the STEM finally achieve what physics has long said was possible, in principle. By far the majority of aberration correctors sold today are for the STEM, and we are seeing continual further developments, applications and improvements in instrument performance. Notable are the increasing use of quantitative imaging to count the number of atoms in a column [135–147]. Mathematical methods are increasingly being used for noise reduction or image reconstruction [148–155] and tilt-series STEM tomography has finally achieved atomic resolution [145,156–159]. Increasingly accurate atomic positions allow ferroelectric properties to be mapped unit cell by unit cell [160–166].

Pixelated detectors seem set to replace the scintillator detector, allowing the imaging mode to be selected after the data has been collected to optimize contrast. In addition, other modes can be constructed such as differential phase contrast to reveal electric or magnetic fields [167] or ptychography [168,169] for high efficiency phase contrast imaging.

Particularly intriguing for me is the possibility offered by depth sectioning with high convergence angles. As the depth resolution goes as the square of the aperture angle, with the 60 mrad probe semiangles being achieved today sub-nm resolution along the beam direction seems to be in reach. The potential is indicated in Fig. 17, where a focal series of the Si (001) surface reconstruction shows that the different layers of the reconstruction can be distinguished clearly [170]. Of course, real microscopes have chromatic aberration which will blur the depth resolution somewhat, and the noise problem may surface again. However, noise reduction techniques should allow a focal series to be acquired in the time normally taken for a single image. It may be that resolution would be improved by tilting off axis, so that atoms do not lie right behind one another. Perhaps we would no longer need to tilt crystals onto a major zone axis. Perhaps we would not need tilting holders, and we could make even smaller gap pole pieces for ultimate resolution.

Even today, it would be fair to argue that the impact of the aberration corrector on the STEM has brought about a transformation of the field of electron microscopy. Indeed, it is bringing about a transformation in the way materials science is undertaken. We are now able to see the complexities of structure and chemistry at the atomic scale like never before, follow and understand the reaction and transformation pathways that create the materials we desire. Such understanding leads to crucial insights into fabricating new devices with improved properties. Trial and error synthesis is being replaced by sound scientific methodology based on informed knowledge of the actual atomistic processes and energy barriers involved.

Truly it has been an exciting and rewarding journey, and one that shows no sign of slowing down in the foreseeable future.

Acknowledgments

The author would like to express his deep thanks to Ondrej Krivanek and the many other colleagues who contributed to the work presented and cited here. The author would like to acknowledge generous funding from the National University of Singapore.

References

[1] S.J. Pennycook, A scan through the history of STEM, in: S.J. Pennycook, P.D. Nellist (Eds.), Scanning Transmission Electron Microscopy, Springer, New York, New York, NY, 2011, pp. 1–90, doi:10.1007/978-1-4419-7200-2_1.
[2] M. von Ardenne, Das Elektronen-Rastermikroskop. Praktische Ausführung, Z. Tech. Phys. 19 (1938) 407–416.
[3] M. von Ardenne, Das Elektronen-Rastermikroskop. Theoretische Grundlagen, Zeit. Physik. 109 (1938) 553–572.
[4] M. Knoll, E. Ruska, Das Elektronenmikroskop, Zeit. Physik. 78 (1932) 318–339.
[5] M. von Ardenne, 4.4 reminiscences on the origins of the scanning electron microscope and the electron microprobe, Adv. Imaging Electron Phys. 96 (1996) 635–652.
[6] A.V. Crewe, A. Crewe, D.N Eggenberger, J. Wall, L. Welter, et al., Electron gun using a field emission source, Rev. Sci. Instrum. 39 (1968) 576–583.
[7] A.V. Crewe, Scanning electron microscopes - is high resolution possible? Science 154 (1966) 729–738.
[8] A.V. Crewe, J. Wall, J. Langmore, Visibility of single atoms, Science 168 (1970) 1338–1340.
[9] A.V. Crewe, High resolution scanning microscopy of biological specimens, Philos. Trans. R. Soc. B. 261 (1971) 61–70.
[10] A. Engel, W. Baumeister, W. Saxton, W.O. Saxton, Mass mapping of a protein complex with the scanning transmission electron microscope, Proc. Nat. Acad. Sci. 79 (1982) 4050.
[11] I.A. Mastrangelo, I. Mastrangelo, P. Hough, P.V.C. Hough, V.G. Wilson, V. Wilson, et al., Monomers through trimers of large tumor antigen bind in region I and monomers through tetramers bind in region II of simian virus 40 origin of replication DNA as stable structures in solution, Proc. Nat. Acad. Sci. U.S.A. 82 (1985) 3626–3630.
[12] G. Sosinsky, N. Francis, D. Derosier, J. Wall, M. Simon, J. Hainfeld, Mass determination and estimation of subunit stoichiometry of the bacterial hook basal body flagellar complex of Salmonella-Typhimurium by scanning-transmission electron-microscopy, Proc. Nat. Acad. Sci. U.S.A. 89 (1992) 4801–4805.
[13] A.M. Donald, A.J. Craven, A study of grain boundary segregation in Cu-Bi alloys using STEM, Philos. Mag. A 39 (1979) 1–11.
[14] C. Humphreys, P. Hirsch, Absorption parameters in electron diffraction theory, Philos. Mag. 18 (1968) 115–122.
[15] A.V. Crewe, J. Langmore, M. Isaacson, Resolution and contrast in the scanning transmission electron microscope, in: Physical Aspects of Electron Microscopy and Microbeam Analysis, 1975, pp. 47–62.
[16] M.M.J. Treacy, A. Howie, C.J. Wilson, Z contrast of platinum and palladium catalysts, Philos. Mag. A. 38 (1978) 569–585.
[17] A. Howie, Image contrast and localized signal selection techniques, J. Microsc. 117 (1979) 11–23.
[18] S.J. Pennycook, L.M. Brown, Cathodoluminescence at dislocations in divalent oxides, J. Lumin. 18-9 (1979) 905–909.
[19] S.J. Pennycook, L.M. Brown, A.J. Craven, Observation of cathodoluminescence at single dislocations by STEM, Philos. Mag. A 41 (1980) 589–600, doi:10.1080/01418618008239335.
[20] S.J. Pennycook, A. Howie, Study of single-electron excitations by electron microscopy II. Cathodoluminescence image contrast from localized energy transfers, Philos. Mag. A. 41 (1980) 809–827, doi:10.1080/01418618008243890.
[21] M.M.J. Treacy, A. Howie, S.J. Pennycook, Z-contrast of supported catalyst particles on the STEM, in: T. Mulvey (Ed.), Electron Microscopy and Analysis, 1979, pp. 261–266.
[22] M.M.J. Treacy, Optimizing atomic-number contrast in annular dark field images of thin-films in the scanning-transmission electron-microscope, J. Microsc. Spectrosc. Electron. 7 (1982) 511–523.
[23] M.M.J. Treacy, J.M. Gibson, On the detection of point-defects in crystals using high-angle diffuse-scattering in the STEM, Inst. Phys. Conf. Ser. No. 61 (1982) 263–266.
[24] M.M.J. Treacy, Imaging with Rutherford scattered electrons in the scanning-transmission electron-microscope, Scanning Electron Microsc. (1981) 185–197.
[25] S.J. Pennycook, J. Narayan, Direct imaging of dopant distributions in silicon by scanning transmission electron microscopy, Appl. Phys. Lett. 45 (1984) 385–387.
[26] S.J. Pennycook, S.D. Berger, R.J. Culbertson, Elemental mapping with elastically scattered electrons, J. Microsc. 144 (1986) 229–249.
[27] S.J. Pennycook, L.A. Boatner, Chemically sensitive structure-imaging with a scanning transmission electron microscope, Nature 336 (1988) 565–567.
[28] J.M. Cowley, Scanning transmission electron microscopy and microdiffraction techniques, Bull. Mater. Sci. 6 (1984) 477–490.
[29] A. Engel, J.W. Wiggins, D.C. Woodruff, A comparison of calculated images generated by six modes of transmission electron microscopy, J. Appl. Phys. 45 (1974) 2739–2747.
[30] S.J. Pennycook, D.E. Jesson, High-resolution incoherent imaging of crystals, Phys. Rev. Lett. 64 (1990) 938–941.
[31] S.J. Pennycook, D.E. Jesson, High-resolution Z-contrast imaging of crystals, Ultramicroscopy 37 (1991) 14–38.
[32] D.E. Jesson, S.J. Pennycook, Incoherent imaging of crystals using thermally scattered electrons, Proc. Roy. Soc. London Ser. A 449 (1995) 273–293.
[33] D.E. Jesson, S.J. Pennycook, Incoherent imaging of thin specimens using coherently scattered electrons, Proc. Roy. Soc. London Ser. A 441 (1993) 261–281.
[34] P.D. Nellist, S.J. Pennycook, Incoherent imaging using dynamically scattered coherent electrons, Ultramicroscopy 78 (1999) 111–124.
[35] P.D. Nellist, P. Nellist, S.J. Pennycook, S. Pennycook, On the origin of transverse incoherence in Z-contrast STEM, J. Electron Microsc. 50 (2001) 227–233.
[36] P.D. Nellist, S.J. Pennycook, The principles and interpretation of annular dark-field Z-contrast imaging, Adv. Imaging Electron Phys. 113 (2000) 147–203.
[37] S.J. Pennycook, S. Pennycook, P. Nellist, P.D. Nellist, Z-contrast scanning transmission electron microscopy, in: D.G. Rickerby, U. Valdrè, G. Valdrè (Eds.), Impact of Electron and Scanning Probe Microscopy on Materials Research, Kluwer, Dordrecht, the Netherlands, 1999, pp. 161–207.

Please cite this article as: S.J. Pennycook, The impact of STEM aberration correction on materials science, Ultramicroscopy (2017), http://dx.doi.org/10.1016/j.ultramic.2017.03.020

[38] O.L. Krivanek, S. Isoda, K. Kobayashi, Lattice imaging of a grain boundary in crystalline germanium, Philos. Mag. 36 (1977) 931–940, doi:10.1080/14786437708239768.
[39] D.E. Jesson, S.J. Pennycook, J. Baribeau, Direct imaging of interfacial ordering in ultrathin $(Si_m\ Ge_n)_p$ superlattices, Phys. Rev. Lett. 66 (1991) 750–753.
[40] S.J Pennycook, M.F. Chisholm, D.E. Jesson, D. Norton, D.H. Lowndes, R. Feenstra, et al., Interdiffusion, growth mechanisms, and critical currents in $YBa_2Cu_3O_{7-x}/PrBa_2Cu_3O_{7-x}$ superlattices, Phys. Rev. Lett. 67 (1991) 765–768.
[41] S.J. Pennycook, M.F. Chisholm, D.E. Jesson, X.Y. Zheng, D.H. Lowndes, Growth and relaxation mechanisms of $YBa_2Cu_3O_{7-x}$ films, Physica C 202 (1992) 1–11.
[42] S.J. Pennycook, N.D. Browning, D.E. Jesson, M.F. Chisholm, A.J. McGibbon, Atomic-resolution imaging and spectroscopy of semiconductor interfaces, Appl. Phys. A. 57 (1993) 385–391.
[43] S.J. Pennycook, N.D. Browning, M.M. McGibbon, A.J. McGibbon, D.E. Jesson, M.F. Chisholm, Direct determination of interface structure and bonding with the scanning transmission electron microscope, Philos. Trans. R. Soc. A 354 (1996) 2619–2634.
[44] N.D. Browning, M.F. Chisholm, S.J. Pennycook, Atomic-resolution chemical analysis using a scanning transmission electron microscope, Nature 366 (1993) 143–146.
[45] P.E. Batson, Simultaneous STEM imaging and electron energy-loss spectroscopy with atomic-column sensitivity, Nature 366 (1993) 727–728.
[46] E.M. James, N.D. Browning, A.W. Nicholls, M. Kawasaki, Y. Xin, S. Stemmer, Demonstration of atomic resolution Z-contrast imaging by a JEOL JEM-2010F scanning transmission electron microscope, J. Electron Microsc. 47 (1998) 561.
[47] O.L. Krivanek, P.H. Gaskell, A. Howie, Seeing order in “amorphous” materials, Nature (1976).
[48] O.L. Krivanek, Method for determining coefficient of spherical aberration from a single electron micrograph, Optik 45 (1976) 97–101.
[49] O.L. Krivanek, J.H. Mazur, The structure of ultrathin oxide on silicon, Appl. Phys. Lett. 37 (1980) 392, doi:10.1063/1.91954.
[50] J. Taftø, O.L. Krivanek, Site-specific valence determination by electron energy-loss spectroscopy, Phys. Rev. Lett. 48 (1982) 560–563.
[51] O.L. Krivanek, C.C. Ahn, R. Keeney, Parallel detection electron spectrometer using quadrupole lenses, Ultramicroscopy 22 (1987) 103–115.
[52] O.L. Krivanek, C. Mory, M. Tence, C. Colliex, EELS quantification near the single-atom detection level, Microsc. Microanal. Microstruct. 2 (1991) 257–267.
[53] O. Scherzer, Sphärische und chromatische Korrektur von Elektronen-Linsen, Optik 2 (1947) 114–132.
[54] O.L. Krivanek, A.J. Gubbens, N. Dellby, C.E. Meyer, Design and 1st applications of a postcolumn imaging filter, Microsc. Microanal. Microstruct. 3 (1992) 187–199, doi:10.1051/mmm:0199200302-3018700.
[55] M. Haider, H. Rose, S. Uhlemann, E. Schwan, B. Kabius, K. Urban, A spherical-aberration-corrected 200 kV transmission electron microscope, Ultramicroscopy 75 (1998) 53–60.
[56] M. Haider, S. Uhlemann, E. Schwan, H. Rose, B. Kabius, K. Urban, Electron microscopy image enhanced, Nature 392 (1998) 768–769.
[57] K.W. Urban, In quest of perfection in electron optics: A biographical sketch of Harald Rose on the occasion of his 80th birthday, Ultramicroscopy 151 (2015) 2–10, doi:10.1016/j.ultramic.2014.12.002.
[58] L.M. Brown, P.E. Batson, N. Dellby, O.L. Krivanek, Brief history of the Cambridge STEM aberration correction project and its progeny, Ultramicroscopy 157 (2015) 88–90, doi:10.1016/j.ultramic.2015.06.006.
[59] P.W. Hawkes, The correction of electron lens aberrations, Ultramicroscopy 156 (2015) A1–A64, doi:10.1016/j.ultramic.2015.03.007.
[60] G. Duscher, N.D. Browning, S.J. Pennycook, Atomic column resolved electron energy-loss spectroscopy, Phys. Status Solidi (a) 166 (1999) 327–342.
[61] P.E. Batson, N. Dellby, O.L. Krivanek, Sub-angstrom resolution using aberration corrected electron optics, Nature 418 (2002) 617–620.
[62] P.D. Nellist, M.F. Chisholm, N. Dellby, O.L. Krivanek, M.F. Murfitt, Z.S. Szilagyi, et al., Direct sub-angstrom imaging of a crystal lattice, Science 305 (2004) 1741.
[63] M. Varela, S.D. Findlay, A.R. Lupini, H.M. Christen, A.Y. Borisevich, N. Dellby, et al., Spectroscopic imaging of single atoms within a bulk solid, Phys. Rev. Lett. 92 (2004) 095502, doi:10.1103/PhysRevLett.92.095502.
[64] S.J. Pennycook, A.R. Lupini, A. Kadavanich, J.R. McBride, S.J. Rosenthal, R.C. Puetter, Aberration-corrected scanning transmission electron microscopy: the potential for nano- and interface science, Z. Metallkd. 94 (2003) 350–357.
[65] P.D. Nellist, S.J. Pennycook, Direct imaging of the atomic configuration of ultradispersed catalysts, Science 274 (1996) 413–415.
[66] K. Sohlberg, S. Rashkeev, A.Y. Borisevich, S.J. Pennycook, S.T. Pantelides, Origin of anomalous Pt-Pt distances in the Pt/alumina catalytic system, ChemPhysChem 5 (2004) 1893–1897, doi:10.1002/cphc.200400212.
[67] N. Shibata, S.J. Pennycook, T.R. Gosnell, G.S. Painter, W.A. Shelton, P.F. Becher, Observation of rare-earth segregation in silicon nitride ceramics at subnanometre dimensions, Nature 428 (2004) 730–733, doi:10.1038/nature02410.
[68] N. Shibata, G.S. Painter, P.F. Becher, S.J. Pennycook, Atomic ordering at an amorphous/crystal interface, Appl. Phys. Lett. 89 (2006) 051908, doi:10.1063/1.2245212.
[69] R. Klie, R.F. Klie, J.P. Buban, J. Buban, M. Varela, A. Franceschetti, et al., Enhanced current transport at grain boundaries in high-T-c superconductors, Nature 435 (2005) 475–478, doi:10.1038/nature03644.
[70] M. Varela, A.R. Lupini, S.J. Pennycook, Z. Sefrioui, J. Santamaria, Nanoscale analysis of $YBa_2Cu_3O_{7-x}/La_{0.67}Ca_{0.33}MnO_3$ interfaces, Solid-State Electronics 47 (2003) 2245–2248, doi:10.1016/S0038-1101(03)00205-3.
[71] M. Varela, T.J. Pennycook, W. Tian, D. Mandrus, S.J. Pennycook, V. Peña, et al., Atomic scale characterization of complex oxide interfaces, J. Mater. Sci. 41 (2006) 4389–4393, doi:10.1007/s10853-006-0150-4.
[72] S.I. Molina, M. Varela, D.L. Sales, T. Ben, J. Pizarro, P.L. Galindo, Direct imaging of quantum wires nucleated at diatomic steps, Appl. Phys. Lett. 91 (2007) 143112.
[73] M. Varela, A.R. Lupini, K. van Benthem, A.Y. Borisevich, M.F. Chisholm, N. Shibata, et al., Materials characterization in the aberration-corrected scanning transmission electron microscope, Annu. Rev. Mater. Res. 35 (2005) 539–569.
[74] S.J. Pennycook, M. Varela, C.J.D. Hetherington, A.I. Kirkland, Materials advances through aberration-corrected electron microscopy, MRS Bull. 31 (2006) 36–43.
[75] S.J. Pennycook, A.R. Lupini, M. Varela, A.Y. Borisevich, M.P. Oxley, M.F. Chisholm, Scanning transmission electron microscopy for nanostructure characterization, in: W. Zhou, Z. Wang (Eds.), Scanning Microscopy for Nanotechnology: Techniques and Applications, Springer, 2007, pp. 152–191.
[76] S.J. Pennycook, M.F. Chisholm, A.R. Lupini, Materials applications of aberration-corrected scanning transmission electron microscopy, Adv. Imaging Electron Phys. (2008), doi:10.1016/s1076-5670(08)01009-4.
[77] A.Y. Borisevich, A.R. Lupini, S.J. Pennycook, Depth sectioning with the aberration-corrected scanning transmission electron microscope, Proc. Nat. Acad. Sci. U.S.A. 103 (2006) 3044–3048.
[78] A.Y. Borisevich, A.R. Lupini, S. Travaglini, S.J. Pennycook, Depth sectioning of aligned crystals with the aberration-corrected scanning transmission electron microscope, Microscopy 55 (2006) 7–12, doi:10.1093/jmicro/dfi075.
[79] K. van Benthem, A.R. Lupini, M. Kim, H.S. Baik, S. Doh, J.-H. Lee, et al., Three-dimensional imaging of individual hafnium atoms inside a semiconductor device, Appl. Phys. Lett. 87 (2005) 034104, doi:10.1063/1.1991989.
[80] K. van Benthem, A.R. Lupini, M.P. Oxley, S.D. Findlay, L.J. Allen, S.J. Pennycook, Three-dimensional ADF imaging of individual atoms by through-focal series scanning transmission electron microscopy, Ultramicroscopy 106 (2006) 1062–1068.
[81] S.N. Rashkeev, S.T. Pantelides, S.J. Pennycook, K. van Benthem, Single Hf atoms inside the ultrathin SiO_2 interlayer between a HfO_2 dielectric film and the Si substrate: How do they modify the interface? Microelectron. Eng. 80 (2005) 416–419, doi:10.1016/j.mee.2005.04.030.
[82] E. Zeitler, Scanning transmission electron microscopy, Optik 31 (1970) 258–280 and 359–366.
[83] J. Cowley, Image contrast in a transmission scanning electron microscope, Appl. Phys. Lett. 15 (1969) 58–59.
[84] S.J. Pennycook, M.F. Chisholm, A.R. Lupini, M. Varela, A.Y. Borisevich, M.P. Oxley, et al., Aberration-corrected scanning transmission electron microscopy: from atomic imaging and analysis to solving energy problems, Philos. Trans. R. Soc. A 367 (2009) 3709–3733, doi:10.1098/rsta.2009.0112.
[85] O.L. Krivanek, P.D. Nellist, N. Dellby, Z. Szilagyi, M.F. Murfitt, Z.S. Szilagyi, Towards sub-0.5 Å electron beams, Ultramicroscopy 96 (2003) 229–237.
[86] M. Watanabe, D.W. Ackland, A. Burrows, C.J. Kiely, D.B. Williams, O.L. Krivanek, et al., Improvements in the X-ray analytical capabilities of a scanning transmission electron microscope by spherical-aberration correction, Microsc. Anal. 12 (2006) 515–526, doi:10.1017/S1431927606060703.
[87] M. Watanabe, X-ray energy-dispersive spectrometry in scanning transmission electron microscopes, in: S.J. Pennycook, P.D. Nellist (Eds.), Scanning Transmission Electron Microscopy, first ed., Springer, 2011, pp. 291–351.
[88] D.A. Muller, L.F. Kourkoutis, M. Murfitt, J.H. Song, H.Y. Hwang, J. Silcox, et al., Atomic-scale chemical imaging of composition and bonding by aberration-corrected microscopy, Science 319 (2008) 1073–1076, doi:10.1126/science.1148820.
[89] H. Sawada, Experimental evaluation of a spherical aberration-corrected TEM and STEM, J. Electron Microsc. 54 (2005) 119–121, doi:10.1093/jmicro/dfi001.
[90] R. Erni, B. Freitag, P. Hartel, H. Müller, P. Tiemeijer, M. van der Stam, et al., Atomic scale analysis of planar defects in polycrystalline diamond, Microsc. Anal. 12 (2006) 492–497.
[91] H. Rose, Phase-contrast in scanning transmission electron microscopy, Optik 39 (1974) 416–436.
[92] S.D. Findlay, N. Shibata, H. Sawada, E. Okunishi, Y. Kondo, T. Yamamoto, et al., Robust atomic resolution imaging of light elements using scanning transmission electron microscopy, Appl. Phys. Lett. 95 (2009) 191913, doi:10.1063/1.3265946.
[93] E. Okunishi, I. Ishikawa, H. Sawada, F. Hosokawa, M. Hori, Y. Kondo, Visualization of light elements at ultrahigh resolution by STEM annular bright field microscopy, Microsc. Microanal. 15 (2009) 164–165, doi:10.1017/S1431927609093891.
[94] S.D. Findlay, N. Shibata, H. Sawada, E. Okunishi, Y. Kondo, Y. Ikuhara, Dynamics of annular bright field imaging in scanning transmission electron microscopy, Ultramicroscopy 110 (2010) 903–923, doi:10.1016/j.ultramic.2010.04.004.
[95] S.D. Findlay, T. Saito, N. Shibata, Y. Sato, J. Matsuda, K. Asano, et al., Direct imaging of hydrogen within a crystalline environment, Appl. Phys. Express 3 (2010) 6603.
[96] R. Ishikawa, E. Okunishi, H. Sawada, Y. Kondo, F. Hosokawa, E. Abe, Direct imaging of hydrogen-atom columns in a crystal by annular bright-field electron microscopy, Nature Mater. 10 (2011) 278–281, doi:10.1038/nmat2957.

Please cite this article as: S.J. Pennycook, The impact of STEM aberration correction on materials science, Ultramicroscopy (2017), http://dx.doi.org/10.1016/j.ultramic.2017.03.020

[97] Q. He, R. Ishikawa, A.R. Lupini, L. Qiao, E.J. Moon, O. Ovchinnikov, et al., Towards 3D mapping of BO_6 octahedron rotations at perovskite heterointerfaces, unit cell by unit cell, ACS Nano. 9 (2015) 8412–8419, doi:10.1021/acsnano.5b03232.
[98] O. Scherzer, The theoretical resolution limit of the electron microscope, J. Appl. Phys. 20 (1949) 20–29.
[99] L. Rayleigh, On the theory of optical images with special reference to the microscope, Philos. Mag 42 (1896) 167–195.
[100] T. Akashi, Y. Takahashi, T. Tanigaki, T. Shimakura, T. Kawasaki, T. Furutsu, et al., Aberration corrected 1.2-MV cold field-emission transmission electron microscope with a sub-50-pm resolution, Appl. Phys. Lett. 106 (2015) 074101, doi:10.1063/1.4908175.
[101] O.L. Krivanek, M.F. Chisholm, V. Nicolosi, T.J. Pennycook, G.J. Corbin, N. Dellby, et al., Atom-by-atom structural and chemical analysis by annular dark-field electron microscopy, Nature 464 (2010) 571–574, doi:10.1038/nature08879.
[102] J. Meyer, A. Chuvilin, G. Algara-Siller, J. Biskupek, U. Kaiser, Selective sputtering and atomic resolution imaging of atomically thin boron nitride membranes, Nano Lett 9 (2009) 2683–2689.
[103] O.L. Krivanek, N. Dellby, M.F. Murfitt, M.F. Chisholm, T.J. Pennycook, K. Suenaga, et al., Gentle STEM ADF imaging and EELS at low primary energies, Ultramicroscopy 110 (2010) 935–945, doi:10.1016/j.ultramic.2010.02.007.
[104] J. Lee, W. Zhou, S.J. Pennycook, J.-C. Idrobo, S.T. Pantelides, Direct visualization of reversible dynamics in a Si_6 cluster embedded in a graphene pore, Nat. Commun. 4 (2013) 1650–1657, doi:10.1038/ncomms2671.
[105] T.J. Pennycook, J.R. McBride, S.J. Rosenthal, S.J. Pennycook, S.T. Pantelides, Dynamic fluctuations in ultrasmall nanocrystals induce white light emission, Nano Lett. 12 (2012) 3038–3042, doi:10.1021/nl3008727.
[106] T.J. Pennycook, L. Jones, H. Pettersson, J. Coelho, Atomic scale dynamics of a solid state chemical reaction directly determined by annular dark-field electron microscopy, Sci. Rep. (2014), doi:10.1038/srep07555.
[107] S.J. Pennycook, W. Zhou, S.T. Pantelides, Watching atoms work: nanocluster structure and dynamics, ACS Nano. 9 (2015) 9437–9440, doi:10.1021/acsnano.5b05510.
[108] J. Lin, O. Cretu, W. Zhou, K. Suenaga, D. Prasai, K.I. Bolotin, et al., Flexible metallic nanowires with self-adaptive contacts to semiconducting transition-metal dichalcogenide monolayers, Nature Nanotechnol. 9 (2014) 436–442, doi:10.1038/nnano.2014.81.
[109] R. Zan, Q.M. Ramasse, U. Bangert, K.S. Novoselov, Graphene reknits its holes, Nano Lett. 12 (2012) 3936–3940, doi:10.1021/nl300985q.
[110] Z. Yang, L. Yin, J. Lee, W. Ren, H.-M. Cheng, H. Ye, et al., Direct observation of atomic dynamics and silicon doping at a topological defect in graphene, Angew. Chem. Int. Ed. 53 (2014) 8908–8912, doi:10.1002/anie.201403382.
[111] Q. Chen, A.L. Koh, A.W. Robertson, K. He, S. Lee, E. Yoon, et al., Rotating anisotropic crystalline silicon nanoclusters in graphene, ACS Nano. 9 (2015) 9497–9506, doi:10.1021/acsnano.5b03476.
[112] S. Jesse, Q. He, A.R. Lupini, D.N. Leonard, M.P. Oxley, O. Ovchinnikov, et al., Atomic-level sculpting of crystalline oxides: toward bulk nanofabrication with single atomic plane precision, Small 11 (2015) 5895–5900, doi:10.1002/smll.201502048.
[113] J. Lin, W. Fang, W. Zhou, A.R. Lupini, J.-C. Idrobo, J. Kong, et al., AC/AB stacking boundaries in bilayer graphene, Nano Lett. 13 (2013) 3262–3268, doi:10.1021/nl4013979.
[114] J. Guo, J. Lee, C.I. Contescu, N.C. Gallego, S.T. Pantelides, S.J. Pennycook, et al., Crown ethers in graphene, Nat. Commun. 5 (2014) 1–6, doi:10.1038/ncomms6389.
[115] X. Zhang, J. Guo, P. Guan, C. Liu, H. Huang, F. Xue, et al., Catalytically active single-atom niobium in graphitic layers, Nat. Commun. 4 (2013) 1924–1927, doi:10.1038/ncomms2929.
[116] W. Zhou, M.D. Kapetanakis, M.P. Prange, S.T. Pantelides, S.J. Pennycook, J.-C. Idrobo, Direct determination of the chemical bonding of individual impurities in graphene, Phys. Rev. Lett. 109 (2012) 206803, doi:10.1103/PhysRevLett.109.206803.
[117] Y. Gong, Z. Liu, A.R. Lupini, G. Shi, J. Lin, S. Najmaei, et al., Band gap engineering and layer-by-layer mapping of selenium-doped molybdenum disulfide, Nano Lett. 14 (2014) 442–449, doi:10.1021/nl4032296.
[118] T.J. Pennycook, M.J. Beck, K. Varga, M. Varela, S.J. Pennycook, S.T. Pantelides, Origin of colossal ionic conductivity in oxide multilayers: interface induced sublattice disorder, Phys. Rev. Lett. 104 (2010) 115901, doi:10.1103/PhysRevLett.104.115901.
[119] T.J. Pennycook, M.P. Oxley, J. Garcia-Barriocanal, F.Y. Bruno, C. Leon, J. Santamaria, et al., Seeing oxygen disorder in YSZ/$SrTiO_3$ colossal ionic conductor heterostructures using EELS, Eur. Phys. J. Appl. Phys. 54 (2011) 33507, doi:10.1051/epjap/2011100413.
[120] J. Gazquez, W. Luo, M.P. Oxley, M. Prange, M.A. Torija, M. Sharma, et al., Atomic-resolution imaging of spin-state superlattices in nanopockets within cobaltite thin films, Nano Lett. 11 (2011) 973–976, doi:10.1021/nl1034896.
[121] M. Varela, J. Gazquez, T.J. Pennycook, M.P. Oxley, S.J. Pennycook, Applications of aberration-corrected scanning transmission electron microscopy and electron energy loss spectroscopy to complex oxide materials, in: S.J. Pennycook, P.D. Nellist (Eds.), Scanning Transmission Electron Microscopy, Springer, 2011, pp. 429–466.
[122] N. Biškup, J. Salafranca, V. Mehta, M.P. Oxley, Y. Suzuki, S.J. Pennycook, S.T. Pantelides, Varela M., Insulating ferromagnetic $LaCoO_{3-\delta}$ films: a phase induced by ordering of oxygen vacancies, Phys. Rev. Lett. 112 (2014) 087202, doi:10.1103/PhysRevLett.112.087202.
[123] C. Li, Y. Wu, T.J. Pennycook, A.R. Lupini, D.N. Leonard, W. Yin, et al., Carrier separation at dislocation pairs in CdTe, Phys. Rev. Lett. 111 (2013) 096403, doi:10.1103/PhysRevLett.111.096403.
[124] C. Li, J. Poplawsky, Y. Wu, A.R. Lupini, A. Mouti, D.N. Leonard, et al., From atomic structure to photovoltaic properties in CdTe solar cells, Ultramicroscopy 134 (2013) 113–125, doi:10.1016/j.ultramic.2013.06.010.
[125] C. Li, Y. Wu, J. Poplawsky, T.J. Pennycook, N. Paudel, W. Yin, et al., Grain-boundary-enhanced carrier collection in CdTe solar cells, Phys. Rev. Lett. 112 (2014) 156103, doi:10.1103/PhysRevLett.112.156103.
[126] R. Ishikawa, R. Mishra, A.R. Lupini, S.D. Findlay, T. Taniguchi, S.T. Pantelides, et al., Direct observation of dopant atom diffusion in a bulk semiconductor crystal enhanced by a large size mismatch, Phys. Rev. Lett. 113 (2014) 155501, doi:10.1103/PhysRevLett.113.155501.
[127] M. Varela, M.P. Oxley, W. Luo, J. Tao, M. Watanabe, A.R. Lupini, et al., Atomic-resolution imaging of oxidation states in manganites, Phys. Rev. B 79 (2009) 085117, doi:10.1103/PhysRevB.79.085117.
[128] M.P. Prange, M.P. Oxley, M. Varela, S.J. Pennycook, S.T. Pantelides, Simulation of spatially resolved electron energy loss near-edge structure for scanning transmission electron microscopy, Phys. Rev. Lett. 109 (2012) 246101, doi:10.1103/PhysRevLett.109.246101.
[129] M.P. Oxley, M.D. Kapetanakis, M.P. Prange, M. Varela, S.J. Pennycook, S.T. Pantelides, Simulation of probe position-dependent electron energy-loss fine structure, Microsc. Anal. 20 (2014) 784–797, doi:10.1017/S1431927614000610.
[130] M.D. Kapetanakis, W. Zhou, M.P. Oxley, J. Lee, M.P. Prange, S.J. Pennycook, et al., Low-loss electron energy loss spectroscopy: an atomic-resolution complement to optical spectroscopies and application to graphene, Phys. Rev. B 92 (2015) 125147, doi:10.1103/PhysRevB.92.125147.
[131] O.L. Krivanek, J.P. Ursin, N.J. Bacon, G.J. Corbin, N. Dellby, P. Hrncirik, et al., High-energy-resolution monochromator for aberration-corrected scanning transmission electron microscopy/electron energy-loss spectroscopy, Philos. Trans. R. Soc. A 367 (2009) 3683–3697, doi:10.1098/rsta.2009.0087.
[132] O.L. Krivanek, T.C. Lovejoy, N. Dellby, T. Aoki, R.W. Carpenter, P. Rez, et al., Vibrational spectroscopy in the electron microscope, Nature 514 (2014) 209–212, doi:10.1038/nature13870.
[133] C. Dwyer, Localization of high-energy electron scattering from atomic vibrations, Phys. Rev. B 89 (2014) 054103, doi:10.1103/PhysRevB.89.054103.
[134] P. Rez, Is localized infrared spectroscopy now possible in the electron microscope? Microsc. Anal. 20 (2014) 671–677, doi:10.1017/S1431927614000129.
[135] V. Ortalan, A. Uzun, B.C. Gates, N.D. Browning, Towards full-structure determination of bimetallic nanoparticles with an aberration-corrected electron microscope, Nat. Nanotechnol. 5 (2010) 843–847, doi:10.1038/nnano.2010.234.
[136] S. Bals, B. Goris, T. Altantzis, H. Heidari, S. Van Aert, G. Van Tendeloo, Seeing and measuring in 3D with electrons, Comptes Rendus Physique 15 (2014) 140–150, doi:10.1016/j.crhy.2013.09.015.
[137] A. De Backer, G.T. Martinez, A. Rosenauer, S. Van Aert, Atom counting in HAADF STEM using a statistical model-based approach: methodology, possibilities, and inherent limitations, Ultramicroscopy 134 (2013) 23–33, doi:10.1016/j.ultramic.2013.05.003.
[138] A. De Backer, A. De wael, J. Gonnissen, S. Van Aert, Optimal experimental design for nano-particle atom-counting from high-resolution STEM images, Ultramicroscopy 151 (2015) 46–55, doi:10.1016/j.ultramic.2014.10.015.
[139] A.J. den Dekker, J. Gonnissen, A. De Backer, J. Sijbers, S. Van Aert, Estimation of unknown structure parameters from high-resolution (S)TEM images: what are the limits? Ultramicroscopy 134 (2013) 34–43, doi:10.1016/j.ultramic.2013.05.017.
[140] R. Ishikawa, A.R. Lupini, S.D. Findlay, S.J. Pennycook, Quantitative annular dark field electron microscopy using single electron signals, Microsc. Anal. 20 (2014) 99–110, doi:10.1017/S1431927613013664.
[141] L. Jones, K.E. MacArthur, V.T. Fauske, A.T.J. van Helvoort, P.D. Nellist, Rapid estimation of catalyst nanoparticle morphology and atomic-coordination by high-resolution Z-contrast electron microscopy, Nano Lett. 14 (2014) 6336–6341, doi:10.1021/nl502762m.
[142] H. Katz-Boon, C.J. Rossouw, C. Dwyer, J. Etheridge, Rapid measurement of nanoparticle thickness profiles, Ultramicroscopy 124 (2013) 61–70, doi:10.1016/j.ultramic.2012.08.009.
[143] J.M. LeBeau, S.D. Findlay, L.J. Allen, S. Stemmer, Standardless atom counting in scanning transmission electron microscopy, Nano Lett. 10 (2010) 4405–4408, doi:10.1021/nl102025s.
[144] G.T. Martinez, A. Rosenauer, A. De Backer, J. Verbeeck, S. Van Aert, Quantitative composition determination at the atomic level using model-based high-angle annular dark field scanning transmission electron microscopy, Ultramicroscopy 137 (2014) 12–19, doi:10.1016/j.ultramic.2013.11.001.
[145] S. Van Aert, K.J. Batenburg, M.D. Rossell, R. Erni, G. Van Tendeloo, Three-dimensional atomic imaging of crystalline nanoparticles, Nature 470 (2012) 374–377, doi:10.1038/nature09741.
[146] S. Van Aert, A. De Backer, G. Martinez, B. Goris, S. Bals, G. Van Tendeloo, et al., Procedure to count atoms with trustworthy single-atom sensitivity, Phys Rev B 87 (2013) 064107, doi:10.1103/PhysRevB.87.064107.
[147] Z.W. Wang, R.E. Palmer, Experimental evidence for fluctuating, chiral-type Au_{55} clusters by direct atomic imaging, Nano Lett. 12 (2012) 5510–5514, doi:10.1021/nl303429z.
[148] A. De Backer, G.T. Martinez, K.E. MacArthur, L. Jones, A. Béché, P.D. Nellist, et al., Dose limited reliability of quantitative annular dark field scanning transmission electron microscopy for nano-particle atom-counting, Ultramicroscopy 151 (2015) 56–61, doi:10.1016/j.ultramic.2014.11.028.

Please cite this article as: S.J. Pennycook, The impact of STEM aberration correction on materials science, Ultramicroscopy (2017), http://dx.doi.org/10.1016/j.ultramic.2017.03.020

[149] L. Jones, H. Yang, T.J. Pennycook, M.S.J. Marshall, S. Aert, N.D. Browning, et al., Smart Align—a new tool for robust non-rigid registration of scanning microscope data, Adv. Struct. Chem. Imaging (2015) 1–16, doi:10.1186/s40679-015-0008-4.
[150] J.C. Meyer, J. Kotakoski, C. Mangler, Atomic structure from large-area, low-dose exposures of materials: a new route to circumvent radiation damage, Ultramicroscopy 145 (2014) 13–21, doi:10.1016/j.ultramic.2013.11.010.
[151] X. Sang, A.A. Oni, J.M. LeBeau, Atom column indexing: atomic resolution image analysis through a matrix representation, Microsc. Anal. 20 (2014) 1764–1771, doi:10.1017/S1431927614013506.
[152] A. Stevens, H. Yang, L. Carin, I. Arslan, N.D. Browning, The potential for Bayesian compressive sensing to significantly reduce electron dose in high-resolution STEM images, Microscopy 63 (2014) 41–51, doi:10.1093/jmicro/dft042.
[153] A.B. Yankovich, B. Berkels, W. Dahmen, P. Binev, S.I. Sanchez, S.A. Bradley, et al., Picometre-precision analysis of scanning transmission electron microscopy images of platinum nanocatalysts, Nat. Commun. 5 (2014) 1–7, doi:10.1038/ncomms5155.
[154] W. Van den Broek, S. Van Aert, D. Van Dyck, A model based reconstruction technique for depth sectioning with scanning transmission electron microscopy, Ultramicroscopy 110 (2010) 548–554, doi:10.1016/j.ultramic.2009.09.008.
[155] W. Van den Broek, A. Rosenauer, S. Van Aert, J. Sijbers, D. Van Dyck, A memory efficient method for fully three-dimensional object reconstruction with HAADF STEM, Ultramicroscopy 141 (2014) 22–31, doi:10.1016/j.ultramic.2014.03.008.
[156] S. Bals, M. Casavola, M.A. Van Huis, S. Van Aert, K.J. Batenburg, G. Van Tendeloo, et al., Three-dimensional atomic imaging of colloidal core–shell nanocrystals, Nano Lett. 11 (2011) 3420–3424, doi:10.1021/nl201826e.
[157] B. Goris, A. De Backer, S. Van Aert, S. Gómez-Graña, L.M. Liz-Marzan, G. Van Tendeloo, et al., Three-dimensional elemental mapping at the atomic scale in bimetallic nanocrystals, Nano Lett. 13 (2013) 4236–4241, doi:10.1021/nl401945b.
[158] M.C. Scott, C.-C. Chen, M. Mecklenburg, C. Zhu, R. Xu, P. Ercius, et al., Electron tomography at 2.4- ångström resolution, Nature 483 (2012) 444–447, doi:10.1038/nature10934.
[159] S. Bals, B. Goris, A. De Backer, S. Van Aert, G. Van Tendeloo, Atomic resolution electron tomography, MRS Bull. 41 (2016) 525–530, doi:10.1557/mrs.2016.138.
[160] A. Borisevich, O.S. Ovchinnikov, H.J. Chang, M.P. Oxley, P. Yu, J. Seidel, et al., Mapping octahedral tilts and polarization across a domain wall in $BiFeO_3$ from Z-Contrast scanning transmission electron microscopy image atomic column shape analysis, ACS Nano. 4 (2010) 6071–6079, doi:10.1021/nn1011539.
[161] A.Y. Borisevich, H.J. Chang, M. Huijben, M.P. Oxley, S. Okamoto, M.K. Niranjan, et al., Suppression of octahedral tilts and associated changes in electronic properties at epitaxial oxide heterostructure interfaces, Phys. Rev. Lett. 105 (2010) 087204, doi:10.1103/PhysRevLett.105.087204.
[162] H.J. Chang, S.V. Kalinin, A.N. Morozovska, Atomically resolved mapping of polarization and electric fields across ferroelectric/oxide interfaces by Z-contrast imaging, Adv. Mater. 23 (2011) 2474–2479, doi:10.1002/adma.201004641.
[163] P. Gao, C.T. Nelson, J.R. Jokisaari, S.-H. Baek, C.W. Bark, Y. Zhang, et al., Revealing the role of defects in ferroelectric switching with atomic resolution, Nat. Commun. 2 (2011) 591–596, doi:10.1038/ncomms1600.
[164] Q. Qiao, Y. Zhang, R. Contreras-Guerrero, R. Droopad, S.T. Pantelides, S.J. Pennycook, et al., Direct observation of oxygen-vacancy-enhanced polarization in a $SrTiO_3$-buffered ferroelectric $BaTiO_3$ film on GaAs, Appl. Phys. Lett. 107 (2015) 201604, doi:10.1063/1.4936159.
[165] C.T. Nelson, B. Winchester, Y. Zhang, S.-J. Kim, A. Melville, C. Adamo, et al., Spontaneous vortex nanodomain arrays at ferroelectric heterointerfaces, Nano Lett. 11 (2011) 828–834, doi:10.1021/nl1041808.
[166] Y.L. Tang, Y.L. Zhu, X.L. Ma, A.Y. Borisevich, A.N. Morozovska, E.A. Eliseev, et al., Observation of a periodic array of flux-closure quadrants in strained ferroelectric $PbTiO_3$ films, Science 348 (2015) 547–551, doi:10.1126/science.1258289.
[167] N. Shibata, S.D. Findlay, Y. Kohno, H. Sawada, Y. Kondo, Y. Ikuhara, Differential phase-contrast microscopy at atomic resolution, Nat. Phys. 8 (2012) 1–5, doi:10.1038/nphys2337.
[168] T.J. Pennycook, A.R. Lupini, H. Yang, M.F. Murfitt, L. Jones, P.D. Nellist, Efficient phase contrast imaging in STEM using a pixelated detector. Part 1: Experimental demonstration at atomic resolution, Ultramicroscopy 151 (2015) 160–167, doi:10.1016/j.ultramic.2014.09.013.
[169] H. Yang, T.J. Pennycook, P.D. Nellist, Efficient phase contrast imaging in STEM using a pixelated detector. Part II: optimisation of imaging conditions, Ultramicroscopy 151 (2015) 232–239, doi:10.1016/j.ultramic.2014.10.013.
[170] R. Ishikawa, A.R. Lupini, Y. Hinuma, S.J. Pennycook, Large-angle illumination STEM: toward three-dimensional atom-by- atom imaging, Ultramicroscopy 151 (2015) 122–129, doi:10.1016/j.ultramic.2014.11.009.
[171] S.J. Pennycook, Transmission electron microscopy, in: F. Bassani, J. Liedl, P. Wyder (Eds.), Encyclopedia of Condensed Matter Physics, Elsevier, 2006, pp. 240–247.

Please cite this article as: S.J. Pennycook, The impact of STEM aberration correction on materials science, Ultramicroscopy (2017), http://dx.doi.org/10.1016/j.ultramic.2017.03.020